Remote Sens. **2014**, *6*, 6283-6299; doi:10.3390/rs6076283

OPEN ACCESS

remote sensing

ISSN 2072-4292

www.mdpi.com/journal/remotesensing

Article

Synthetic Aperture Radar (SAR) Interferometry for Assessing Wenchuan Earthquake (2008) Deforestation in the Sichuan Giant Panda Site

Fulong Chen [1,2,*], Huadong Guo [1,2], Natarajan Ishwaran [2], Wei Zhou [1,2], Ruixia Yang [1,2], Linhai Jing [1], Fang Chen [1] and Hongcheng Zeng [3]

[1] Key Laboratory of Digital Earth Science, Institute of Remote Sensing and Digital Earth, Chinese Academy of Sciences, No. 9 Dengzhuang South Road, Beijing 100094, China; E-Mails: guohd@radi.ac.cn (H.G.); zhouwei@radi.ac.cn (W.Z.); yangrx@radi.ac.cn (R.Y.); jinglh@radi.ac.cn (L.J.); chenfang@radi.ac.cn (F.C.)

[2] International Centre on Space Technologies for Natural and Cultural Heritage under the Auspices of UNESCO, No. 9 Dengzhuang South Road, Beijing 100094, China; E-Mail: ishgaja@gmail.com

[3] Faculty of Forestry, University of Toronto, 33 Willcocks Street, Toronto, ON M5S 3B3, Canada; E-Mail: hongcheng.zeng@utoronto.ca

***** Author to whom correspondence should be addressed; E-Mail: chenfl@radi.ac.cn; Tel.: +86-10-8217-8198; Fax: +86-10-8217-8915.

Received: 5 March 2014; in revised form: 26 June 2014 / Accepted: 2 July 2014 / Published: 4 July 2014

Abstract: Synthetic aperture radar (SAR) has been an unparalleled tool in cloudy and rainy regions as it allows observations throughout the year because of its all-weather, all-day operation capability. In this paper, the influence of Wenchuan Earthquake on the Sichuan Giant Panda habitats was evaluated for the first time using SAR interferometry and combining data from C-band Envisat ASAR and L-band ALOS PALSAR data. Coherence analysis based on the zero-point shifting indicated that the deforestation process was significant, particularly in habitats along the Min River approaching the epicenter after the natural disaster, and as interpreted by the vegetation deterioration from landslides, avalanches and debris flows. Experiments demonstrated that C-band Envisat ASAR data were sensitive to vegetation, resulting in an underestimation of deforestation; in contrast, L-band PALSAR data were capable of evaluating the deforestation process owing to a better penetration and the significant coherence gain on damaged forest areas. The percentage of damaged forest estimated by PALSAR decreased from 20.66% to 17.34% during 2009–2010, implying an approximate 3% recovery rate of forests in the earthquake

impacted areas. This study proves that long-wavelength SAR interferometry is promising for rapid assessment of disaster-induced deforestation, particularly in regions where the optical acquisition is constrained.

Keywords: SAR interferometry; coherence; Wenchuan Earthquake; giant panda habitat

1. Introduction

Interferometric synthetic aperture radar (InSAR) or differential interferometric synthetic aperture radar (DInSAR) is a quantitative tool for DEM generation [1,2], change detection [3] and surface displacement monitoring [4,5]. In general, coherence is the basis of InSAR applications. In other words, high coherence simplifies phase unwrapping procedures and enhances the reliability of derived DEMs or displacements in DInSAR approaches. Different from optical remote sensing, synthetic aperture radar (SAR) actively transmits signals and then receives backscattering of observed scenarios. This operational mode is effective in all-weather conditions and throughout day and night; it makes SAR remote sensing a significantly advantageous tool in cloudy and rainy regions either for part of or throughout the year. Nowadays, applications of SAR remote sensing have been expanded to cover a number of study areas owing to the occurrence of multi-mode SAR data, e.g., multi-temporal, band, resolution, angle as well as polarization. Among them, natural and cultural heritage monitoring is one promising field, either from aspects of SAR amplitude change detection [6], polarimetric analysis [7] or interferometry preventive diagnostics [8].

As one of the well-known global icons of biodiversity conservation, the giant panda is listed on CITES Appendix I and is an endangered species included in the Red List of the World Conservation Union (IUCN) [9]. At present, the species is restricted to only 20 or so isolated patches of mountain-forests at the edge of the Tibetan plateau, distributed across Sichuan, Shaanxi and Gansu provinces of China. The largest concentrations of the giant pandas are in the Sichuan province. The Sichuan Giant panda Sanctuaries, a 924,500 ha area including the Wolong Biosphere Reserve, was declared a UNESCO World Heritage site in 2006. Wolong is considered to be the home of the largest concentration of wild giant pandas; about 100–150 animals inhabit this reserve.

On 12 May 2008, the Wenchuan Earthquake (magnitude 8.0) struck the Sichuan province, and two mountain ranges inhabited by giant pandas, the Minshan and Qionglai, were seriously impacted. In order to investigate the panda habitat response to this disaster, several studies have been conducted, either through field surveys [10,11] or using remote sensing tools [12]. Although these studies are significant for the ongoing habitat restoration plans as well as long-term conservation, they have two major drawbacks with regard to use in future natural disaster events in Sichuan (a province that is most vulnerable to earthquakes): firstly, field surveys are limited by difficult access to giant panda habitats even during normal times, and accessibility is worsened in the aftermath of an earthquake; second, remote sensing studies dependent solely on optical images suffer from poor visibility in the cloudy-rainy climate of Sichuan (the rainy season spans from May to September). These constraints result in incomplete data acquisition and biased estimates of key parameters.

Nowadays, an abundance of different change detection approaches based on SAR remote sensing has been developed. They can be divided into five categories: differential method [13,14], statistical testing method [15], model method [16], coherence method [17,18] and other integrated methods [19,20]. In order to overcome the constraints of field surveys and optical remote sensing mentioned above, in this study, the coherence approach was applied for assessing Wenchuan Earthquake (2008) deforestation in the Sichuan Giant panda site. The performance of C-band Envisat ASAR and L-band ALOS PALSAR data was further compared, and the result implied the potential of long-wavelength SAR interferometry for the evaluation of disaster-induced deforestation.

2. Study Site and Experimental Data

Taking Minshan and Qionglai mountains in Sichuan, China, as the study site (see Figure 1), the impact of Wenchuan Earthquake on panda habitats was evaluated by means of multi-mode SAR data (C-band Envisat ASAR and L-band ALOS PALSAR). The deep south-west of Minshan and deep north-east of Qionglai mountains were jointly covered by the swath of Envisat ASAR and ALOS PALSAR. Interferometric coherence analysis was used as a quantitative tool to evaluate the influence of the natural disaster on habitats within the World Heritage site. The epicenter of the Wenchuan Earthquake was not too far from the Wolong Biosphere Reserve (see Figure 1). The Caopo Reserve further north of the earthquake epicenter (Figure 1) is also part of the Sichuan Giant Panda Sanctuaries World Heritage site.

Figure 1. Study area of Minshan and Qinglai mountains jointly covered by the Envisat ASAR (highlighted by red) and ALOS PALSAR (highlighted by white) satellites in Sichuan, China. The white star, quite close to the Wolong Biosphere Reserve, is the location of the epicenter of the earthquake.

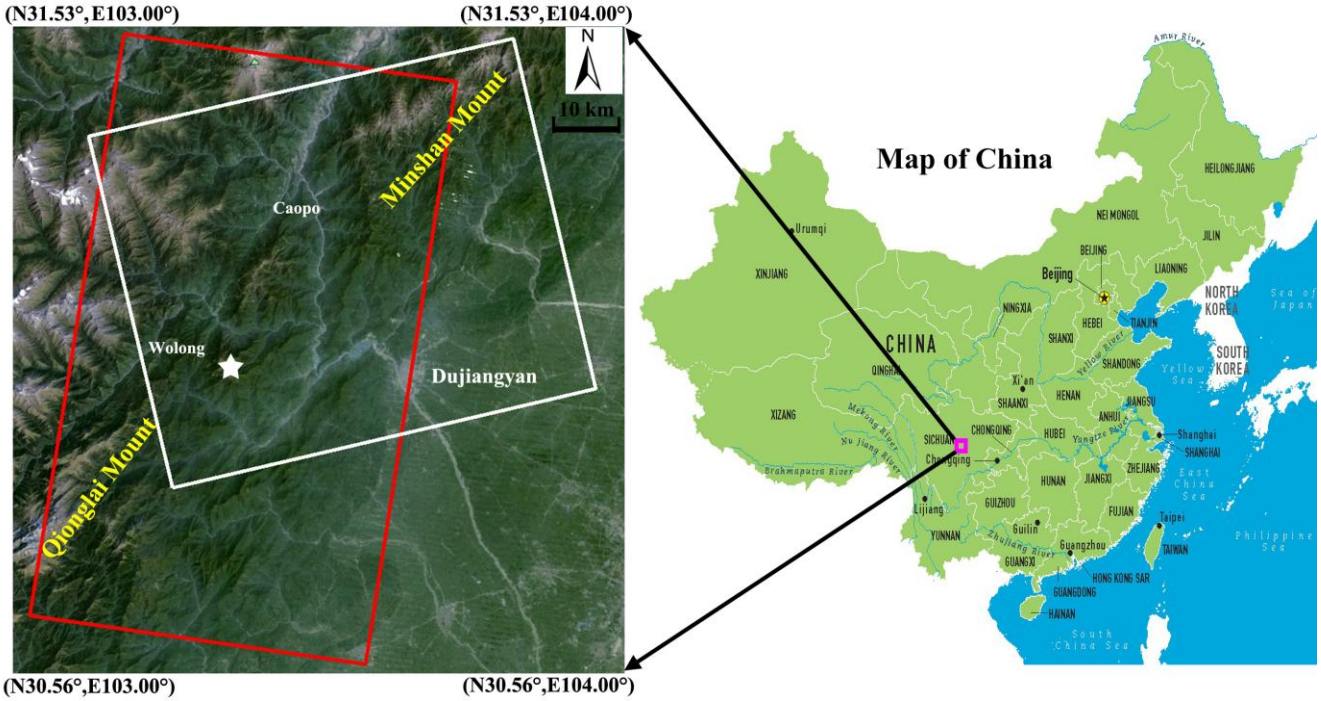

Twenty-four scenes of Envisat ASAR single look complex (SLC) and 17 scenes of ALOS PALSAR SLC images were employed for SAR interferometry analysis. C-band (5.6 cm wavelength) ASAR data, track 290 with descending mode, were acquired for the period from 24 December 2007 to 30 August 2010. The corresponding incidence angle was approximately 23°, resulting in 20 meters ground resolution. L-band (23.6 cm wavelength) ALOS PALSAR data, ascending mode with an incidence angle of 34°, were acquired for the period from 2 February 2007 to 29 December 2010. PALSAR has two fine acquisition modes including Fine Beam Single-polarization (FBS, range bandwidth of 28 MHz) in HH polarization and Fine Beam Dual-polarization (FBD, 14 MHz) in HH/HV dual polarization, respectively. The range bands overlap fully due to the same center frequency, permitting interferometric processing of mixed FBS-FBD pairs with common HH polarization (FBD data need to be doubly oversampled to preserve approximately 8 meters ground resolution). The 3 arc-second (~90 m) shuttle radar topography mission (SRTM) DEM data from the United States Geological Survey (USGS) were used for topographic phase estimation in the first step, and then for InSAR products' geocoding (transforming Range-Doppler coordinates into Universal Transverse Mercator map geometry system).

3. Coherence for the Deforestation Monitoring and Assessment

Due to their proximity to the epicenter (the star in Figure 1), the landscape over Minshan and Qionglai mountain habitats changed significantly due to earthquake-induced landslides, mantle stripping and infrastructure collapse. The disaster-triggered deforestation has worsened the prevalent fragmentation trend within and in the areas surrounding the Wolong Biosphere Reserve. In this study, inspired by the work of Bouaraba *et al*. [21], the coherence analysis was conducted for the deforestation monitoring on the earthquake impacted areas. In general, de-correlation occurs on vegetation areas because of volume scattering. When the forest is damaged by a natural disaster, interferometric coherence of exposed regions would rise significantly. This fact could serve as the basis for deforestation analysis. Due to the combination of co-registration challenge and severe temporal de-correlation, the quality of interferogram generated from cross-event acquisitions is always low, preventing the information extraction related to deforestation. To minimize the difference of geometry and time parameters, the selection of interferometric image pairs became the key issue. The following three criteria were proposed for coherence image generation: (i) the absolute spatial-temporal baselines of pre- and post-event interferograms are similar in order to minimize the influences that may arise due to the use of different baselines; (ii) the small baseline strategy is applied to generate high-quality interferograms for comparison; (iii) the acquisition seasons of compared interferometric image-pairs are same in order to minimize the seasonal de-correlation effect.

Coherent change detection was conducted by comparing images between pre- and post-event periods; and a zero-point shifting approach was proposed to analyze the differential coherence image. We assume that for a natural-random evolution process, the histogram plot of differential coherence image follows a zero-peaking Gaussian distribution; that is, the zero-point line is at the 50% mark in the histogram plot, equally dividing the coherence loss and gain. However, this assumption would be broken by external-impact trends either from natural disasters or anthropogenic activities, resulting in a phenomenon called zero-point shifting. This phenomenon was used for the deforestation quantitative assessment caused by the external driving force of Wenchuan Earthquake using generated differential coherence images spanning pre- and post-event observations.

4. Results

4.1. Deforestation Monitoring by Envisat ASAR

The small baseline criterion "ii" (smaller than 250 m spatially and 180 days temporally) was applied for the interferogram generation, resulting in a total of 49 interferograms (Figure 2). Only one pre-event interferogram was obtained comprising of acquisitions of 24 December 2007 and 3 March 2008. For simplification, the data acquisition was formatted as year-month-day in Arabic numerals. The pre-event interferogram was thus renamed as 20080303-20071224 (normal baseline 26.18 m, temporal baseline 70 days, spring-winter season combination). The selection of post-event interferograms was further carried out using the criteria of similar baseline and same acquisition (criteria "i" and "iii"), in addition to the small baseline criterion; that is, firstly, candidate post-event interferograms should be located in the defined normal baseline range ([−40, 40] m highlighted in cyan in Figure 2) and have a uniform temporal arm-length (70 days) comparable to the pre-event interferogram of 20080303-20071224; second, the consistent spring-winter season combination should be ensured in candidate post-event interferograms. The post-event interferogram of 20090112-20081103 (perpendicular baseline 17.33 m, temporal baseline 70 days) was then selected for the coherence comparison (Figure 3). From the comparison, it is clear that the coherence along the Min River has increased remarkably because of forest damage. A loss of coherence was detected in the bottom-right portion of the post-event image and could be attributed to anthropogenic activities such as residential areas, cultivated land and river beaches in the fluvial plain as well as to temporal variation of soil humidity (see Figure 3).

Figure 2. Interferogram formation of Envisat ASAR based on the small baseline strategy (smaller than 250 m spatially and 180 days temporally). The searching range for candidate post-event interferograms is highlighted in cyan. Selected pre- and post-event interferograms are marked by pink lines.

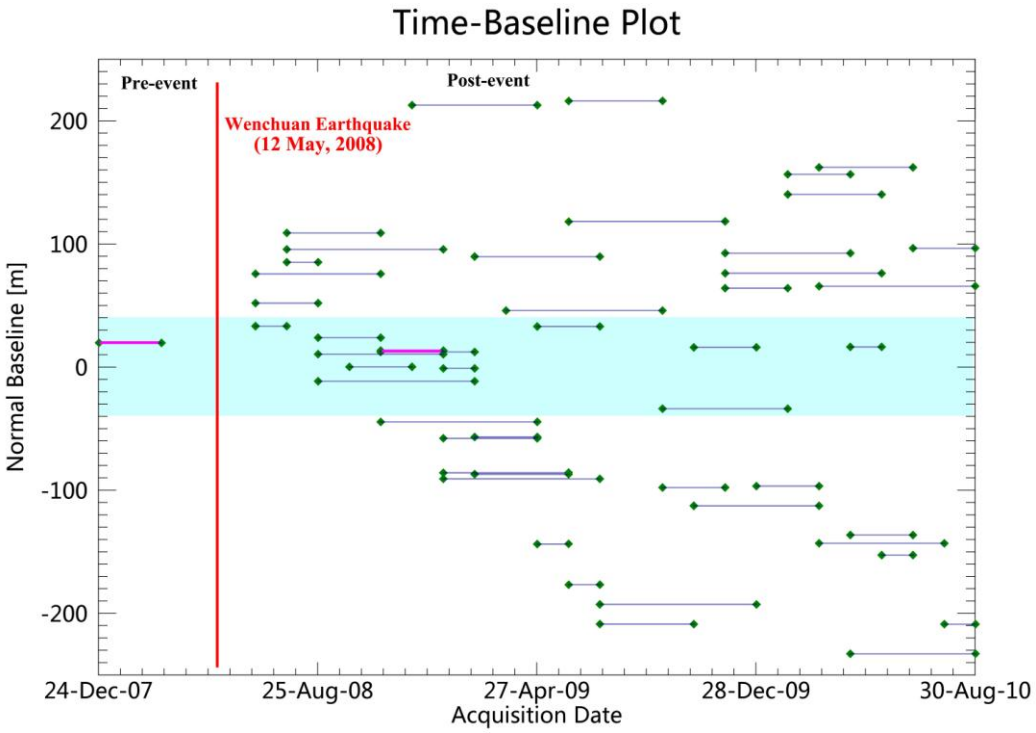

Figure 3. Coherence images of (**a**) 20080303-20071224 (pre-event), (**b**) 20090112-20081103 (post-event) using Envisat ASAR data; red ellipses in (a) and (b) indicate the prominent coherence gain induced by the earthquake; (**c**) the fluvial plain includes residence (marked by pink polygons), cultivated land (marked by green polygons) and river beaches (marked by blue polygons).

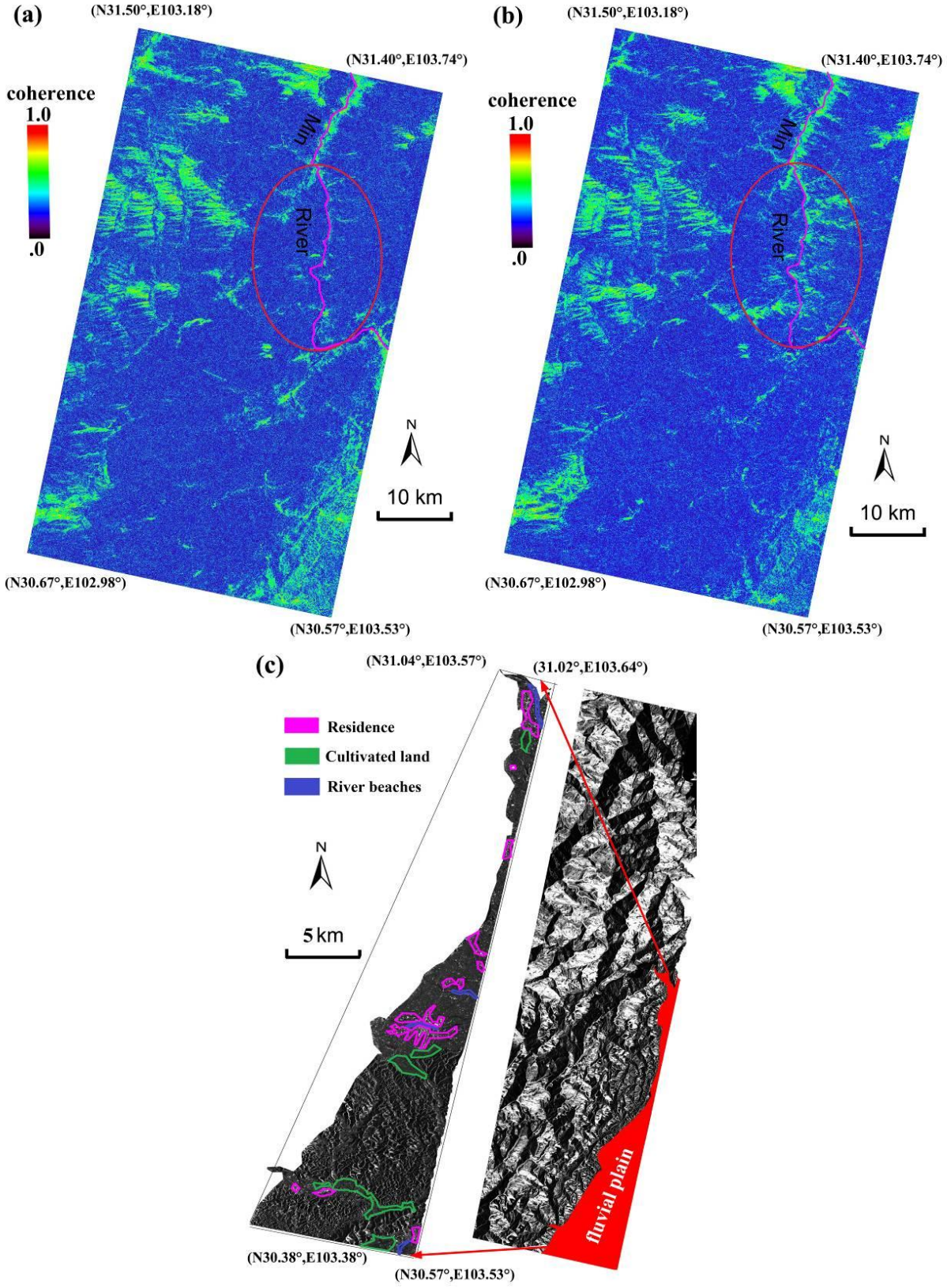

4.2. Deforestation Monitoring by ALOS PALSAR

Due to its long wavelength, L-band ALOS PALSAR has a better penetration. The deforestation process could be precisely detected owing to the significant coherence gain on damaged vegetation areas. Taking advantage of this possibility, we applied PALSAR data for quantitative analysis of deforestation. Analogous to the Envisat ASAR data processing, the small baseline criterion "ii" (smaller than 2000 m spatially and 322 days temporally) was firstly employed to generate 48 initial interferograms, as illustrated in Figure 4.

Figure 4. Interferogram formation of ALOS PALSAR based on the small baseline strategy (smaller than 2000 m spatially and 322 days temporally). The searching range for candidate pre- and post-event interferograms is highlighted in cyan, and the selected interferograms for analysis are marked by pink lines.

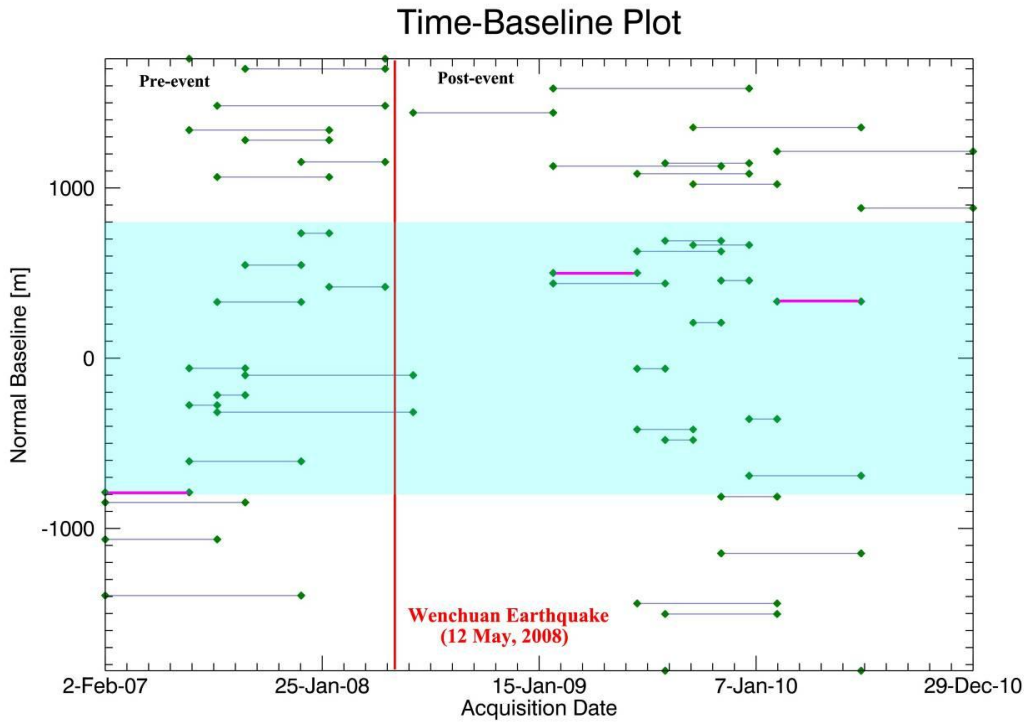

In order to further mitigate the de-correlation induced by normal baselines, a rigorous threshold (−800, 800 m) was applied for the candidate interferogram selection, resulting in a searching zone highlighted in cyan (Figure 4). There was only one interferogram for 2010, that is, 20100628-20100210 (summer-winter combination, 563m normal baseline and 138 days interval, so-called interferogram 2010). For the purpose of multi-temporal analysis, it was used as the reference for the selection of other pre- and post-event interferograms. Obeying the criteria of similar baseline and same acquisition (criteria "i" and "iii"), the pre-event interferogram of 20070620-20070202 (summer-winter combination, −746 m normal baseline and 138 days interval, so-called interferogram 2007), and the post-event interferogram of 20090625-20090207 (summer-winter combination, 755 m perpendicular baseline and 138 days interval, so-called interferogram 2009) were selected, respectively. The three selected interferograms in the year of 2007, 2009 and 2010 are highlighted in pink in Figure 4. Their coherence images were then

generated, as shown in Figure 5, demonstrating the coherence gain trend on loss of forest areas caused by the landslides, avalanches and debris flows resulting from the earthquake.

Figure 5. Coherence images of (**a**) 20070620-20070202 (pre-event), (**b**) 20090625-20090207 (post-event after one year recovery) and (**c**) 20100628-20100210 (two year recovery) using ALOS PALSAR data; red ellipses indicate the prominent coherence gain induced by the earthquake.

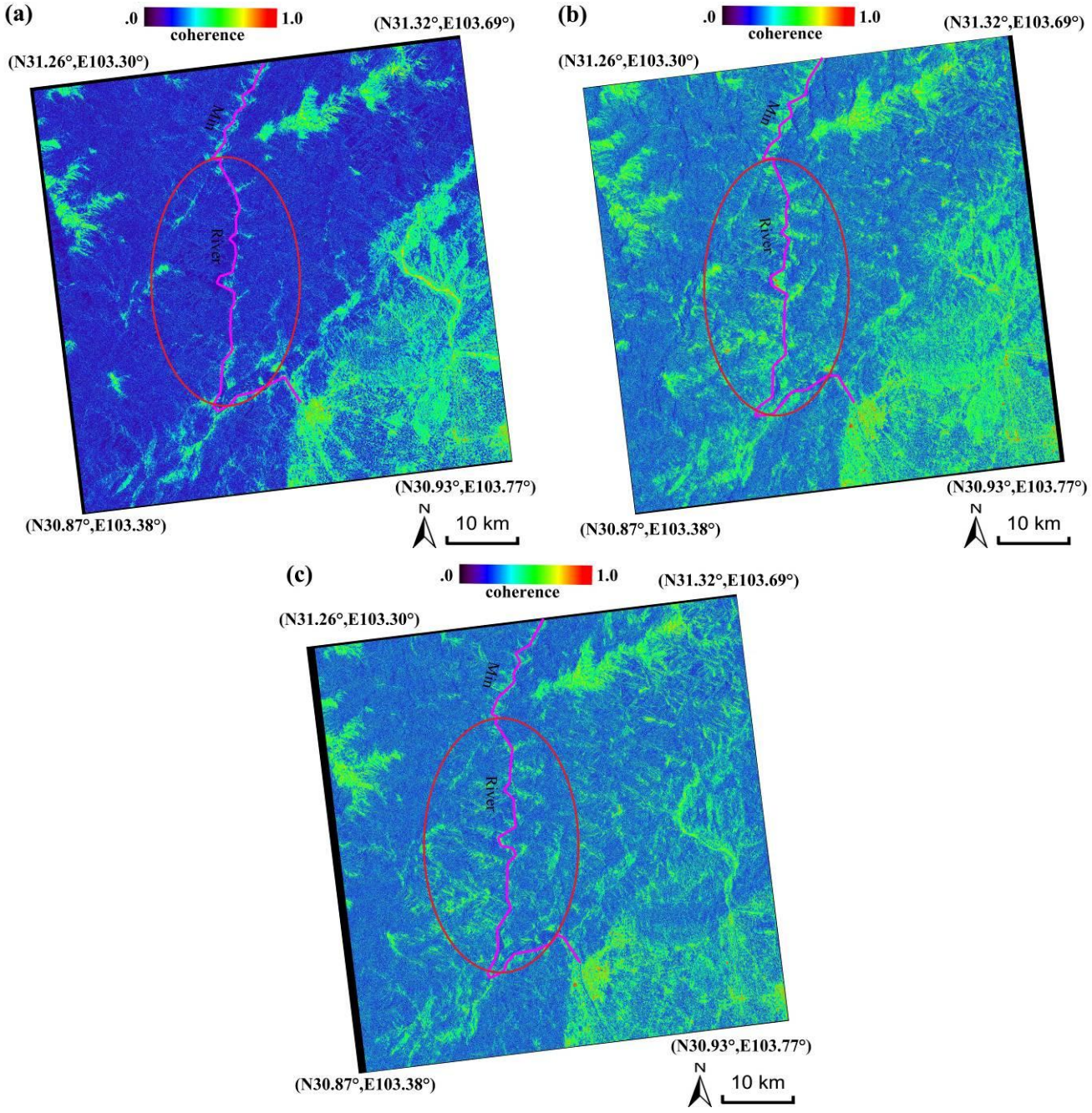

The seismic intensity of the earthquake in the study site was in the range of VII–XI Chinese seismic intensity [22]. Characterized by rugged topography, steep high mountains, deep valleys and complicated geological structures, a great number of landslides and rock avalanches were triggered, particularly in Gaojianggou, Shaofanggou, Hongcungou, and Yinxinggou regions. The landslide-induced deforestation

in this site included [23]: (1) landslides triggered by the main earthquake and aftershocks, which were responsible for tree destruction along their run-out paths; (2) increased erosion and debris flow triggered by heavy rainfalls on slopes with unconsolidated mantles. After that, differential coherence images were generated, including images for 2009–2007 and 2010–2007, as illustrated in Figure 6. Apart from deforestation, there are other coherence loss/gain areas, e.g., gain in residential zones caused by artificial post-constructions (marked by red polygons), and loss in river beaches or low-lying areas caused by soil humidity variations (marked by blue polygons).

Figure 6. Coherence loss (dark color, marked by blue polygons) and gain (light color, marked by red polygons) areas in differential coherence images except for deforestation, (**a**) PALSAR image of 2009–2007 and (**b**) PALSAR image of 2010–2007; sub-images of "1, 2 and 3" in (a) and (b) highlight the coherence loss and gain in detail.

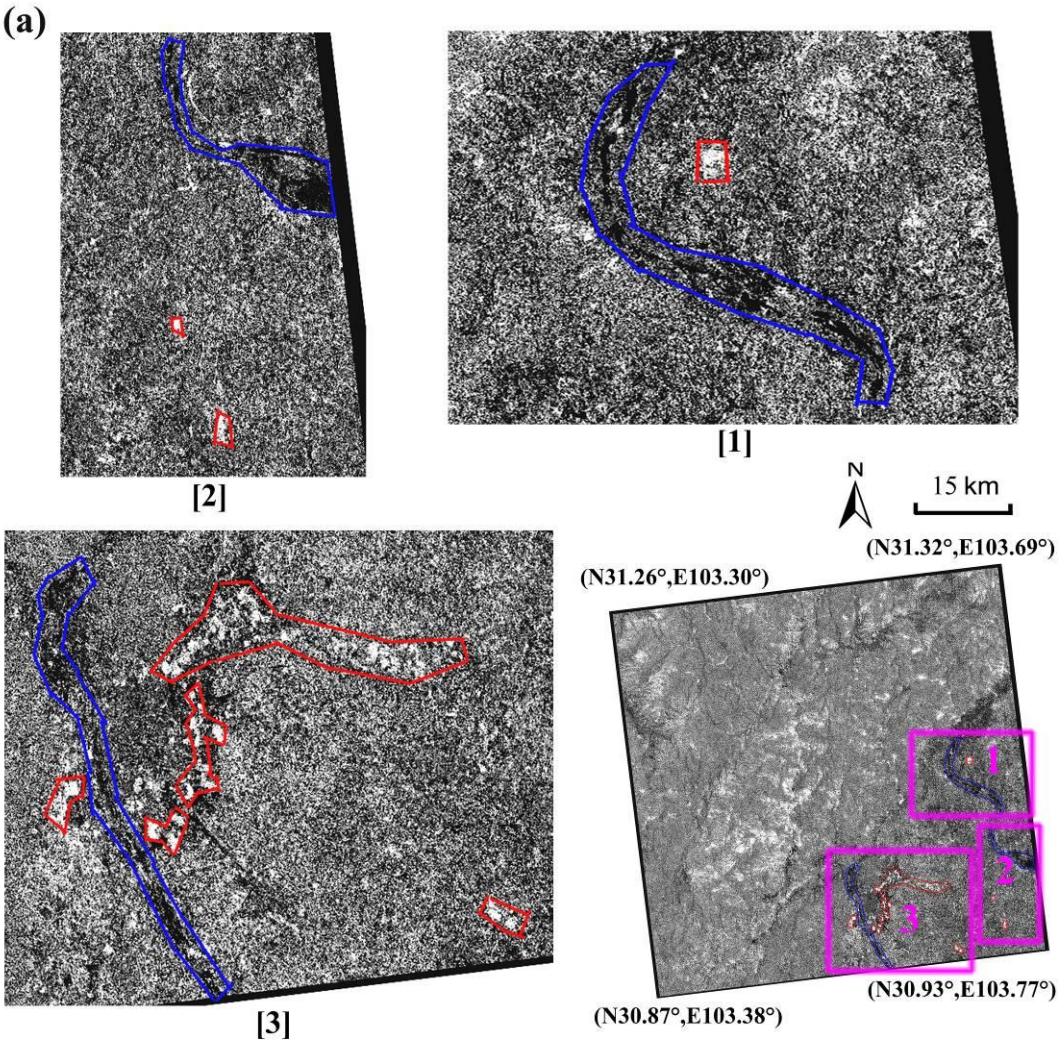

Figure 6. *Cont.*

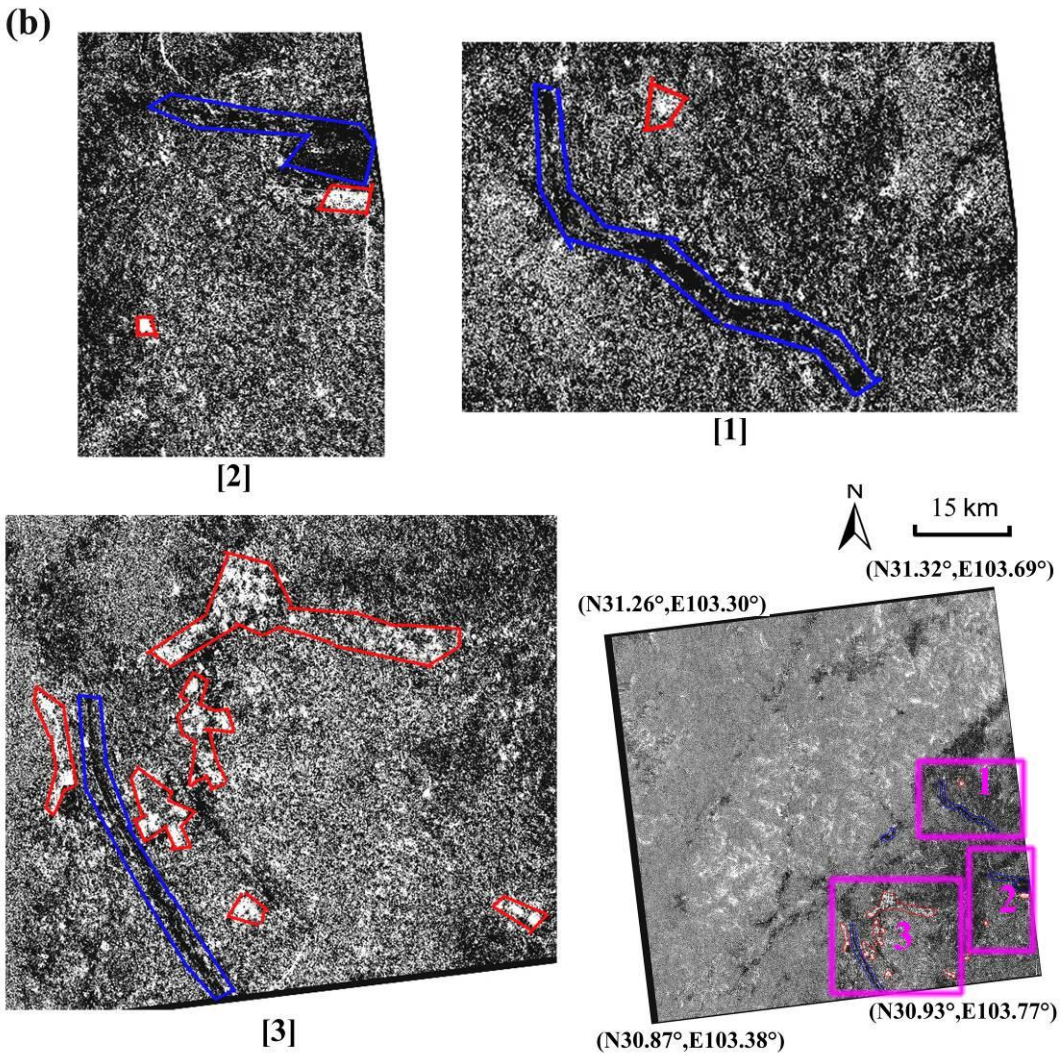

4.3. Quantitative Assessment and Cross Comparison

In order to exclude impacts from fluvial plains (no relationship with deforestation), masks were first applied on differential coherence images; then the percentages of destroyed forest were quantitatively estimated by the zero-point shifting on histogram plots of C-band Envisat ASAR (see Figure 7) and L-band PALSAR data (see Figure 8), respectively. For the histogram plot of Envisat ASAR data (the differential coherence image was generated by subtracting the pre-event coherence image of 20080303-20071224 from the post-event coherence image of 20090112-20081103), the zero-point line lies at 47.96%, indicating that only 2.04% of the forest in the observed scenario was destroyed (Figure 7). In contrast, using the differential coherence images of ALOS PALSAR in the period of 2009–2007 and 2010–2007 (Figure 8), the zero-point line is at 29.34%, demonstrating that 20.66% of the forest was either destroyed or had not yet recovered up until the year 2009 (Figure 8a); the portion of damaged forest shrunk to 17.34% (50.0–32.66) in 2010 (Figure 8b), implying an approximate recovery of 3% in a year. This low recovery rate (3%) could be attributed to physical degradation of slopes. During the earthquake, slopes in many of the areas illustrated by the images in

Figure 5, particularly steep slopes approaching rivers or streams, became barren and rocky after their soil mantle was ripped out.

Figure 7. Phenomenon of zero-point shifting in the histogram plot of Envisat ASAR differential coherence image (derived by coherence images of 20080303-20071224 and 20090112-20081103); zero-point line is at 47.96% indicating an estimated deforestation of 2.04%.

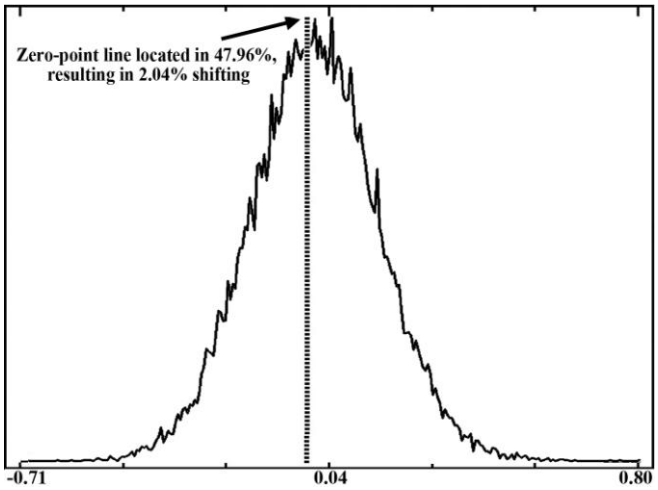

Figure 8. Phenomena of zero-point shifting in the histogram plot of PALSAR differential coherence images; (**a**) the histogram plot of differential coherence image 2009–2007, (**b**) the histogram plot of differential coherence image 2010–2007. Zero-point line in (a) is at 29.34%, indicating a that 20.66% forest was either destroyed or had not yet recovered up until the year 2009; in (b) the portion of damaged forest shrunk to 17.34% (50.0–32.66) in 2010, indicating approximately 3% recovery during 2008–2009.

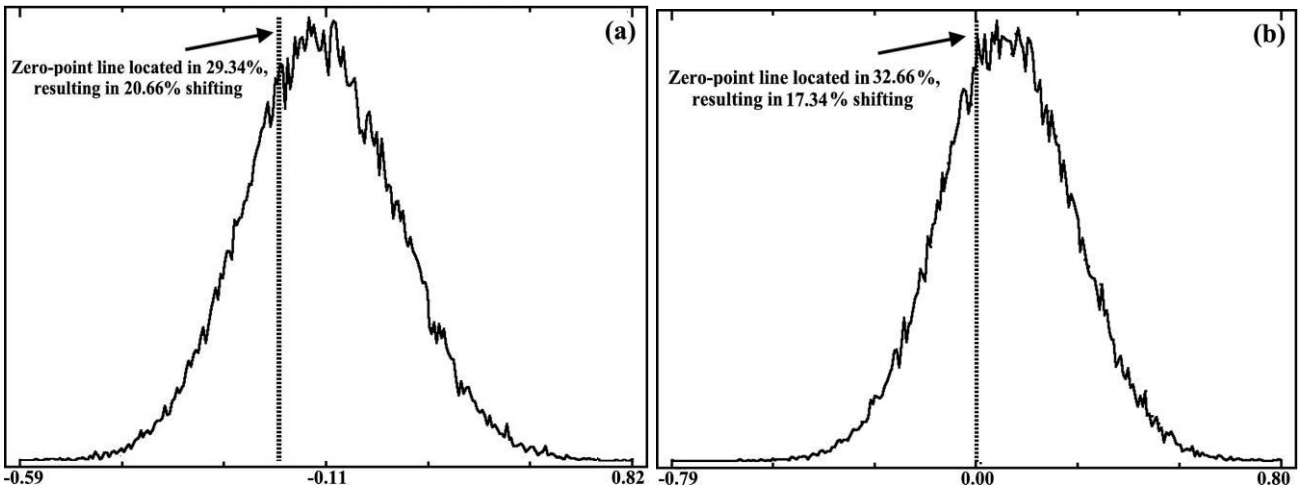

The inconsistency in the estimates of Envisat ASAR and ALOS PALSAR could be due to the three following reasons. Firstly, the spatial coverage of the two datasets is different (see Figure 1), introducing various coherence gain and loss from non-overlapped regions. Second, the temporal parameters of coherence images (e.g., temporal baselines and acquisition seasons) of Envisat ASAR and ALOS PALSAR data are varying. Last but not least, the capability of coherence maintenance of two datasets is

different. Generally, C-band Envisat ASAR data are sensitive to vegetation. Except for degraded bare slopes, sparse vegetation remained on moderate-to-mildly damaged regions, resulting in omitted detections due to severe de-correlation. Furthermore, the signature of disaster-induced deforestation could also be hampered by the random variation of coherence gain and loss. Two factors mentioned above jointly determine an underestimation of the disaster-induced deforestation by Envisat ASAR data, e.g., 2.04% in this study. In contrast, the limitation could be overcome by L-band ALOS PALSAR owing to a longer wavelength and significant coherence gains on damaged forest regions. Consequently, PALSAR data are more suitable for quantitative assessment of deforestation using InSAR approaches. In this study, PALSAR detected 20.66% of deforestation induced by the earthquake.

5. Validation and Discussion

In the past five years, two field investigations (in the year of 2009 and 2013, respectively) were conducted for the deforestation monitoring. The earthquake-induced deforestation was considerable particularly in slopes along the Min River from Yingxiu to Wenchuan Country (as highlighted by the red ellipses in Figures 3 and 5) due to landslides or debris flows. The surface of those slopes has been ripped out, leaving barren or rocky mantles, as illustrated by the field photo in Figure 9. Generally, saturated water content, capillary moisture capacity, field water capacity, total porosity and capillary porosity were lower in the landslide impacted regions [10]. The degraded soil condition was reflected in the low recovery rate of forest.

It was assumed that the coherence gain is an evidence for deforestation. To back up this assumption, a mosaic of airborne optical images along Min River was acquired in 2011 (c) and used for the PALSAR InSAR-derived results validation through comparisons with the coherence images of 20070620-20070202 ((a) pre-event) and 20100628-20100210 ((b) post-event), as illustrated in Figure 10. Two observations should be emphasized: (1) in the pre-event image, high coherence only occurs in residential areas or in barren surface; however, the coherence increases significantly after the earthquake, particularly on slopes where the forest has been destroyed; (2) the spatial pattern of high-coherence in the post-event image is consistent with deforested areas (showing as exposed surface) in the airborne optical image. Boxes “1” and “2” in Figure 10 illustrated the disaster-induced deforestation in detail using detected anomalies of coherence as well as land cover change. As a quantitative analysis, 100 random sampling points were extracted from coherence image of 20100628-20100210 and the airborne optical image. Deforested points in the coherence image were validated by manual interpretation on the optical image, indicating classification accuracy up to 82% (note that the two images have the same geographical coordinate system after geo-coding). The mismatch between deforested points in coherence and optical images could be due to the following reasons: firstly, the spatial resolution of the two sets of data is different, *i.e.*, 8 m of coherence image *vs*. 2 m of optical image. In addition, the imaging geometry is also different, slant looking of SAR (resulting in foreshortening, layover and shadow in SAR products) *vs*. centrally projected sensors in the optical image. Finally, there is a temporal gap between coherence and optical images, introducing differences in vegetation cover.

Figure 9. A field photo of barren and rocky surface-cover on a landslide impacted region along the Min River in Wenchuan Country, Sichuan prov., China.

Fortunately, results indicated that severe damage only occurred on unsuitable or marginally-suitable habitat regions represented in steep slope with few bamboo distributions; this finding was consistent with that of Zheng *et al*. [11]. An IUCN monitoring mission undertaken during 12–17 April 2010 at the request of the World Heritage Committee of UNESCO also confirmed that impact of the earthquake was largely concentrated in the northeast corner of the World Heritage site, e.g., Wolong Reserve, and that only a small amount of bamboo forest was affected. While no major change to the feeding habitat of giant pandas occurred, heavily impacted areas, where soils and ground cover were ripped out, would nevertheless have restricted or caused shifts to the normal movement patterns of pandas. Furthermore, considering the accompanying occurrence of bamboos and arbores (e.g., bamboo tends to grow beneath the canopy of arbores), the disaster-induced deforestation has changed the flora ecosystem (e.g., the growth and propagation of bamboo forests), which in turn influences the short-term feeding capability of giant panda habitats.

Generally, there are two limitations of SAR remote sensing for the surveillance application of panda habitats: (1) habitats run across Sichuan, Shaanxi and Gansu provinces. The spatial coverage of satellites (one frame) prevents the monitoring and a systematic analysis of the entire habitat. In this study, for example, only a portion of Minshan and Qionglai Mount nearby the epicenter was

investigated. Although the study was representative for the assessment of the most earthquake-impacted zone, the extent of fragmentation and isolation of habitats between the area of study and nearby areas could not be evaluated. (2) Data requisition is another hindering factor. Selecting interferometric pairs to mitigate the difference from spatial-temporal baselines as well as acquisition seasons was a considerably difficult task, requiring abundance of repeat-cycle SAR archival data. Furthermore, short wavelength SAR data (C-band) are challenging for monitoring densely vegetated habitats because of severe de-correlation and significant underestimation.

Figure 10. InSAR-derived deforestation of PALSAR ((**a**) pre-event image of 20070620-20070202, (**b**) post-event image of 20100628-20100210) compared with the airborne optical image ((**c**) acquired in 2011). Boxes "1" and "2" represent areas with significant deforestation.

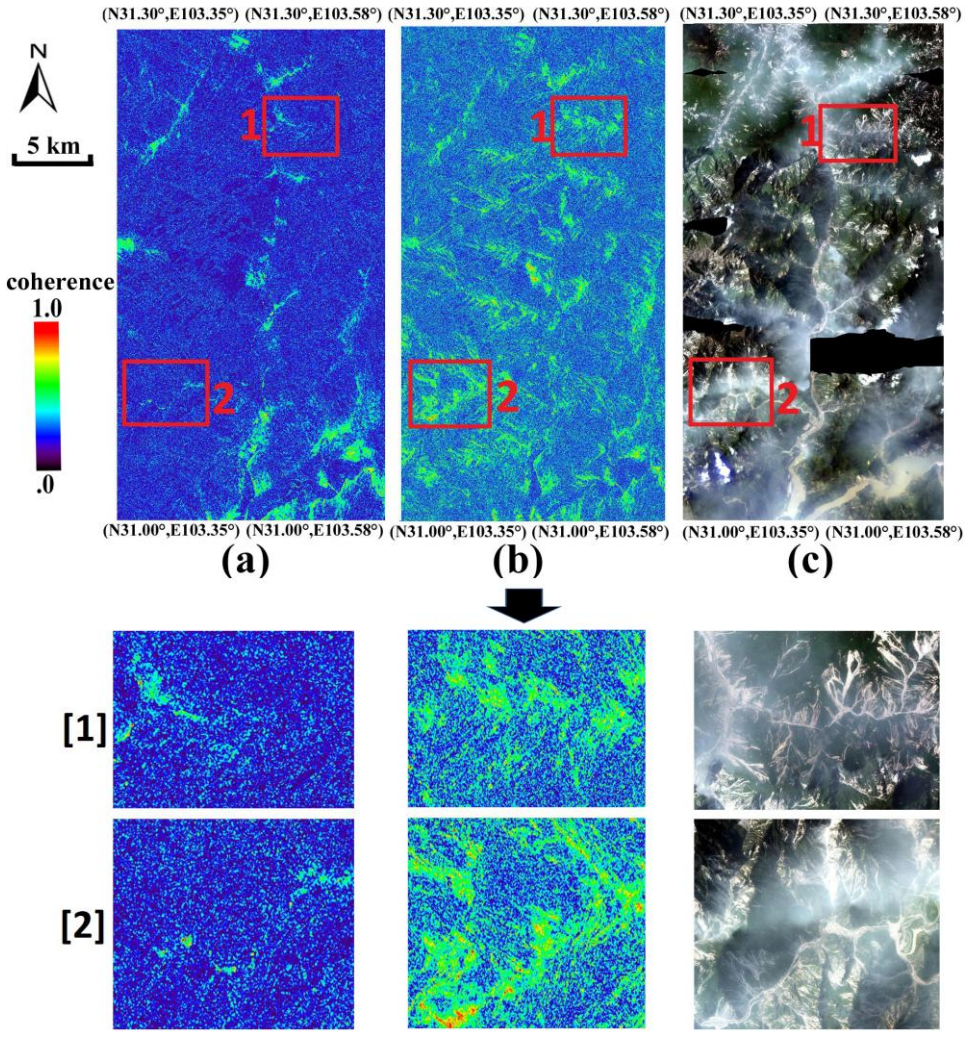

6. Conclusions

For the first time, this paper has shown a deforestation monitoring approach by means of InSAR tools for giant panda habitats within the Sichuan Giant Panda Habitats World Heritage site and the broader Minshan and Qionglai Mountain areas following the Wenchuan Earthquake of 2008. Coherence analysis from C- and L-band SAR data demonstrated that the disaster-induced deforestation

was significant (20.66% destroyed as estimated by PALSAR), particularly along the Min River approaching the epicenter, and was interpreted from the extent of vegetation deterioration from landslides, avalanches and debris flows. Comparison of InSAR-derived results demonstrated that L-band ALOS PALSAR data have a better performance for the deforestation assessment than C-band Envisat ASAR data owing to the significant coherence gain on damaged areas, which was also validated by field investigations and analysis carried out using optical airborne images. Quantitative analysis of PALSAR based on the zero-point shifting method indicated that the forest recovery after the disaster was relatively slow, *i.e.*, 3% during 2009–2010; where the soil layer had been ripped out by the earthquake and slopes became bare rock, colonization by vegetation would take a much longer time than deforested areas where the soil layer was still largely intact. This study implied the potential of SAR interferometry for deforestation assessment in regions that are vulnerable to natural disasters.

Acknowledgments

This work was supported by funding from the International S&T Cooperation Program of China (2013DFG21640), Hundred Talents Program of the Institute of Remote Sensing and Digital Earth, Chinese Academy of Sciences (Y2ZZ27101B), and National Natural Science Foundation of China (41201455). ENVISAT ASAR, ALOS PALSAR data are copyrighted by the European Space Agency and the Japan Aerospace Exploration Agency, respectively.

Author Contributions

Fulong Chen did the coherence analysis for the earthquake-induced deforestation evaluation. He together with Huadong Guo, Natarajan Ishwaran, Wei Zhou and Ruixia Yang conducted the field investigation for results validation. Linhai Jing, Fang Chen and Hongcheng Zeng did SAR products geo-coding. All the authors contributed to developing the ideas presented and the writing of the paper.

Conflicts of Interest

The authors declare no conflict of interest.

References and Notes

1. Baselice, F.; Ferraioli, G.; Pascazio, V. DEM reconstruction in layover areas from SAR and auxiliary input data. *IEEE Geosci. Remote Sens. Lett.* **2009**, *6*, 253–257.
2. Zebker, H.A.; Villasenor, J. Decorrelation in interferometric radar echoes. *IEEE Trans. Geosci. Remote Sens.* **1992**, *30*, 950–959.
3. Preiss, M.; Gray, D.A.; Stacy, N.J.S. Detecting scene changes using synthetic aperture radar interferometry. *IEEE Trans. Geosci. Remote Sens.* **2006**, *44*, 2041–2054.
4. Chen, F.L.; Lin, H.; Zhou, W.; Hong, T.H.; Wang, G. Surface deformation detected by ALOS PALSAR small baseline SAR interferometry over permafrost environment of Beiluhe section, Tibet Plateau, China. *Remote Sens. Environ.* **2013**, *138*, 10–18.
5. Lu, Z.; Rykhus, R.; Masterlark, T.; Dean, K.D. Mapping recent lava flows at Westdahl volcano, Alaska, using radar and optical satellite imagery. *Remote Sens. Environ.* **2004**, *91*, 345–353.

6. Cigna, F.; Tapete, D.; Lasaponara, R.; Masini, N. Amplitude change detection with Envisat ASAR to image the cultural landscape of the Nasca Region, Peru. *Archaeol. Propect.* **2013**, *20*, 117–131.
7. Stewart, C.; Lasaponara, R.; Schiavon, G. ALOS PALSAR analysis of the archaeological site of Pelusium. *Archaeol. Propect.* **2013**, *20*, 109–116.
8. Tapete, D.; Fanti, R.; Cecchi, R.; Petrangeli, P.; Casagli, N. Satellite radar interferometry for monitoring and early-stage warning of structural instability in archaeological sites. *J. Geophys. Eng.* **2012**, *9*, 10–25.
9. IUCN. *IUCN Red List of Threatened Species*; IUCN: Gland, Switzerland, 2008. Available online: www.incnredlist.org (accessed on 16 October 2013).
10. Cheng, S.; Yang, G.; Yu, H.; Li, J.; Zhang, L. Impacts of Wenchuan earthquake-induced landslides on soil physical properties and tree growth. *Ecol. Indic.* **2012**, *15*, 263–270.
11. Zheng, W.; Xu, Y.; Liao, L.; Yang, X.; Gu, X.; Shang, T.; Ran, J. Effect of the Wenchuan earthquake on habitat use patterns of the giant panda in the Minshan Mountains, southwestern China. *Biol. Conserv.* **2012**, *145*, 241–245.
12. Xu, W.; Wang, X.; Ouyang, Z.; Zhang, J.; Li, Z.; Xiao, Y.; Zheng, H. Conservation of giant panda habitat in south Minshan, China, after the May 2008 earthquake. *Front. Ecol. Environ.* **2009**, *7*, 353–358.
13. Cable, J.W.; Kovacs, J.M.; Shang, J.; Jiao, X. Multi-temporal polarimetric RADARSAT-2 for land cover monitoring in northeastern Ontario, Canada. *Remote Sens.* **2014**, *6*, 2372–2392.
14. Gong, M.; Li, Y.; Jiao, L.; Jia, M.; Su, L. SAR change detection based on intensity and texture changes. *ISPRS J. Photogramm. Remote Sens.* **2014**, *93*, 123–135.
15. Tourneret, J.; Doisy, M.; Lavielle, M. Bayesian off-line detection of multiple change-points corrupted by multiplicative noise: Application to SAR image edge detection. *Signal Proc.* **2003**, *83*, 1871–1887.
16. Huang, S.; Cai, X.; Chen, S.; Liu, D. Change detection method based on fractal model and wavelet transform for multitemporal SAR images. *Int. J. Appl. Earth Obs. Geoinf.* **2011**, *13*, 863–872.
17. Wdowinski, S.; Kim, S.; Amelung, F.; Dixon, T.H.; Miralles-Wilhelm, F.; Sonenshein, R. Space-based detection of wetlands' surface water level changes from L-band SAR interferometry. *Remote Sens. Environ.* **2008**, *112*,681–696.
18. Meyer, F.J.; Sandwell, D.T. SAR interferometry at Venus for topography and change detection. *Planet. Space Sci.* **2012**, *73*, 130–144.
19. Shang, R.; Qi, L.; Jiao, L.; Stolkin, R.; Li, Y. Change detection in SAR images by artificial immune multi-objective clustering. *Eng. Appl. Artif. Intell.* **2014**, *31*, 53–67.
20. Schmitt, A.; Wessel, B.; Roth, A. An innovative curvelet-only-based approach for automated change detection in multi-temporal SAR imagery. *Remote Sens.* **2014**, *6*, 2435–2462.
21. Bouaraba, A.; Younsi, A.; Belhadj-Aissa, A.; Acheroy, M.; Milisavljevic, N.; Closson, D. Robust techniques for coherent change detection using COSMO-SkyMed SAR images. *Prog. Electromagn. Res.* **2012**, *22*, 219–232.
22. Guo, D.; Hamada, M. Qualitative and quantitative analysis on landslide influential factors during Wenchuan earthquake: A case study in Wenchun County. *Eng. Geol.* **2013**, *152*, 202–209.

23. Ouimet, W.B. Landslides associated with the May 12, 2008 Wenchuan earthquake: Implications for the erosion and tectonic evolution of the Longmen Shan. *Tectonophysics*. **2010**, *491*, 244–252.